Experimental investigation of airflow and heat transfer by natural convection in an insulated box with a Phase Change Material using a Particle Image Velocimetry technique

Tanathep Leungtongkum, Onrawee Laguerre, Denis Flick, Alain Denis, Steven Duret, Nattawut Chaomuang

Experimental investigation of airflow and heat transfer by natural convection in an insulated box with a Phase Change Material using a Particle Image Velocimetry technique

Tanathep Leungtongkum, Onrawee Laguerre, Denis Flick, Alain Denis, Steven Duret, Nattawut Chaomuang

PII: S0260-8774(22)00261-8

DOI: https://doi.org/10.1016/j.jfoodeng.2022.111207

Reference: JFOE 111207

To appear in: *Journal of Food Engineering*

Received Date: 10 March 2022

Revised Date: 27 June 2022

Accepted Date: 1 July 2022

Please cite this article as: Leungtongkum, T., Laguerre, O., Flick, D., Denis, A., Duret, S., Chaomuang, N., Experimental investigation of airflow and heat transfer by natural convection in an insulated box with a Phase Change Material using a Particle Image Velocimetry technique, *Journal of Food Engineering* (2022), doi: https://doi.org/10.1016/j.jfoodeng.2022.111207.

Credit Author Statement

Author's name	**Contributions**
Tanathep Leungtongkum	Conceptualization, Methodology, Investigation, Validation, Formal analysis, Software, Writing - Original Draft Preparation, Visualization.
Onrawee Laguerre	Validation, Formal analysis, Writing - Review & Editing, Supervision, Project Administration, Funding acquisition.
Denis Flick	Methodology, Validation, Formal analysis, Writing - Review & Editing, Supervision.
Steven Duret	Validation, Formal analysis, Writing - Review & Editing, Supervision.
Alain Denis	Investigation, Software.
Nattawut Chaomuang	Conceptualization, Methodology, Investigation, Validation, Formal analysis, Software, Writing - Original Draft Preparation, Visualization, Funding acquisition.

Experimental investigation of airflow and heat transfer by natural convection in an insulated box with a Phase Change Material using a Particle Image Velocimetry technique

Tanathep Leungtongkum[a], Onrawee Laguerre[a], Denis Flick[b], Alain Denis[a], Steven Duret[a] and Nattawut Chaomuang[c]*

[a]Université Paris-Saclay, INRAE, FRISE, 92761 Antony, France

[b]Université Paris-Saclay, INRAE, AgroParisTech, UMR SayFood, 91300 Massy, France

[c]Department of Food Engineering, School of Engineering, King Mongkut's Institute of Technology Ladkrabang, Bangkok, Thailand 10520

***Corresponding author:** Nattawut Chaomuang, Tel: +66 (0) 2 329 8356 Ext. 21, e-mail: nattawut.ch@kmitl.ac.th

Abstract

Airflow and heat transfer via natural convection in an insulated box with Phase Change Material (PCM) were experimentally investigated using Particle Image Velocimetry (PIV) and temperature measurements. The effects of PCM positions (side wall and lid) on flow pattern and temperature distribution were studied under empty and loaded conditions. Two loads were considered to study the obstacle effect and the influence of heat exchange with air. When PCM was either at the side wall or at the lid of the box, laminar flow was observed and the corresponding Rayleigh number was about 10^7. Upward flow was always observed near the side walls of the box. When PCM was on the side, downward flow occurred along the PCM; in the empty case, flow was almost 2D but became 3D when the load was added. When PCM was on the lid, the air cooled in contact with PCM, detached from it and flowed downwards. In the

empty case, downward flow was unstable, and with the load, it followed preferential pathways. The type of load exerted little effect on flow patterns at thermal steady state. Thus, a simpler load (extruded polystyrene) can be used in the first approach. The maximum velocity was about 0.1 $m \cdot s^{-1}$, so free convection cannot be neglected compared with conduction. Regarding temperature performance, PCM on the side and on the lid showed no substantial difference if gaps were left between the load and the walls or PCM.

Keywords: Airflow, Heat Transfer, Natural convection, Insulated box, Phase Change Material

Nomenclature

A	Aspect ratio [-]
c_p	Specific heat [$J \cdot kg^{-1} \cdot K^{-1}$]
g	Acceleration due to gravitation [$m \cdot s^{-2}$]
Gr	Grashof number [-]
H	Height [m]
L	Length [m]
Ra	Rayleigh number [-]
Pr	Prandtl number [-]
t	Time [s]
T	Temperature [°C or K]
ΔT	Temperature difference [°C or K]
U	Overall heat transfer coefficient [$W \cdot m^{-2} \cdot K^{-1}$]
v	Velocity magnitude [$m \cdot s^{-1}$]
W	Width [m]
x, y, z	Coordinates [m]

Greek letters

α	Thermal diffusivity [$m^2 \cdot s^{-1}$]
β	Thermal expansion coefficient [K^{-1}]
λ	Thermal conductivity [$W \cdot m^{-1} \cdot K^{-1}$]
ε	Emissivity [-]
ρ	Density [$kg \cdot m^{-3}$]
μ	Dynamic viscosity [$kg \cdot m^{-1} \cdot s^{-1}$]
υ	Kinematic viscosity [$m^2 \cdot s^{-1}$]

Subscripts

a	air
c	cold
g	glass
h	hot
s	surface
th	thermal
w	wall
∞	free stream

Abbreviations

CFD	Computational Fluid Dynamics
PCM	Phase Change Material
PIV	Particle Image Velocimetry
TYL	Tylose
XPS	Extruded Polystyrene

1. Introduction

Insulated boxes equipped with Phase Change Material (PCM) have been widely used in the transport of various temperature-sensitive products such as meat and fishery products (Paquette et al., 2017), fruit and vegetables (Zhao et al., 2019), and pharmaceutical products (Robertson et al., 2017). The advantages of insulated boxes with PCM include low investment and operating costs, flexibility in storage temperatures and volumes, and ease of maintenance (Zhao et al., 2020). However, two drawbacks emerge: the temperature in an insulated box is difficult to control, and temperature heterogeneity is often observed, with a low temperature in the vicinity of the PCM and a high temperature further away from the PCM (Laguerre et al., 2008a; Margeirsson et al., 2012; Navaranjan et al., 2013). This problem can result in the degradation of product quality, for instance chilling/freezing injury (a temperature that is too low leads to cell damage) and pose a safety risk (a temperature that is too high leads to bacterial growth) (Laguerre et al., 2019). As reviewed by Leungtongkum et al. (2021), numerous experimental and numerical studies have been conducted to evaluate the thermal performance of insulated boxes equipped with PCM. Choi and Burgess (2007) developed simplified heat transfer models based on an ice melting test for the estimation of heat flow resistance (R-value) which is a factor generally used to determine the insulation performance of the box. Later, Singh et al. (2008) applied this method and reported the R-values of insulated boxes made of various insulating materials with different wall thicknesses and box dimensions. Various 2D and 3D Computational Fluid Dynamics (CFD) models of insulated boxes with PCM were developed to study the influences of different factors on the evolution of air/product temperatures (Du et al., 2020; Laguerre et al., 2019; Laguerre et al., 2018; Margeirsson et al., 2012; Paquette et al., 2017; Xiaofeng and Xuelai, 2021). These factors included box characteristics (dimensions, shape of inner corners, types and thicknesses of insulating materials, internal surface emissivity), PCMs (types, mass, and position in a box), products (types, initial temperature, mass, and arrangement in a box), and operating conditions (ambient temperature and transport

duration) (Leungtongkum et al., 2021). To reduce computational time, analytical and zonal models were also developed as a complementary approach (East et al., 2009; Laguerre et al., 2019; Laguerre et al., 2018). These models enable useful information (e.g., PCM melting duration and product temperature change during shipment) to be acquired as a function of the box design and usage conditions. Xiaofeng and Xuelai (2021) developed an insulated box with multiple partitions for delivery of various products, which require different preservation temperatures (ambient, chilled, and frozen temperatures) in the same box. Despite these efforts, there is still no universal optimal condition that can be applied to control the air/product temperatures in an insulated box.

All heat transfer modes can occur simultaneously in an insulated box with PCM: conduction (inside the product, PCM and the walls of the box), natural convection (between air and product/PCM in the box), natural/forced convection (between external air and the box), and radiation (between the walls and product/PCM in the box) (Leungtongkum et al., 2021). For model simplification, most numerical studies consider heat transfer by conduction, and sometimes also by radiation, while natural convection inside the box tends to be neglected (Du et al., 2020). In fact, all heat transfer modes can be of the same order of magnitude, and natural convection can exert significant impacts, especially on temperature heterogeneity in the insulated box (Laguerre and Flick, 2010).

Natural convection in closed cavities occurs in a wide range of engineering applications and has been extensively studied with both experimental and numerical approaches (Miroshnichenko and Sheremet, 2018; Pandey et al., 2019). The configurations commonly studied are air or water in a rectangular cavity of which two opposite (horizontal/vertical) walls are maintained at different constant and uniform temperatures (hot and cold) while the other walls are perfectly insulated (adiabatic). Many studies also introduce porous medium or solid

objects (flat plate, cylinder and sphere) in the cavity to observe their effects on heat transfer and airflow (Ataei-Dadavi et al., 2019; Lee et al., 2016). The knowledge acquired using a cavity filled with porous media can be applied to the case of small products such as cereal grains (ratio between characteristic lengths of product and cavity ≤ 0.02). However, the models are limited in the case of larger products (e.g., meat, fruit and vegetables) where the ratio is much higher (> 0.1) (Laguerre et al., 2008b). Moreover, the configuration of a product-loaded insulated box with PCM is more complex because all walls are subjected to heat loss and the wall equipped with PCM (cold wall) has a non-uniform temperature as PCM melts more rapidly at some positions (Jevnikar and Siddiqui, 2019). Several experimental and numerical studies were conducted to investigate heat transfer and airflow in air-filled cavities with PCM at one wall. Aitlahbib and Chehouani (2015) developed a two-dimensional numerical model to evaluate the thermal performance of an insulated container with one vertical wall equipped with PCM, the opposite one kept at higher temperature while other walls were well-insulated. The results demonstrated that the container with PCM wall achieved superior thermal performance than the one without. The same cavity configuration was numerically studied by Labihi et al. (2017). The effect of volume expansion of the PCM during solidification was considered in the model. Better predictions were obtained when this effect was taken into account. Moreno et al. (2020) developed a transient 2D-CFD model to describe the airflow and the heat transfer in an air-filled cavity with a PCM wall. The numerical results revealed flow patterns similar to ones observed in experiment during melting process. The temperature stratification was intensified after the liquid fraction of the PCM started to predominate ($> 50\%$). Orozco et al. (2021) further performed a numerical study with the same cavity configuration but this time the PCM wall was segmented into small volumes. The results showed that the segmentation of the PCM wall had no significant effect on the flow patterns and the temperature distributions in the air-filled cavity. Both flow topology and temperature stratification in the cavity with the segmented PCM

144 wall were similar to those in the cavity with the non-segmented PCM wall. However, for the
145 same requirement of thermal retention duration, the amount of the PCM could be reduced by
146 dividing the PCM container into segments. These mentioned studies essentially dedicated to
147 the use of PCM to enhance the energy efficiency of buildings. Only the temperature
148 measurements were used for the model validation (no air velocity measurement). To our best
149 knowledge, no experimental studies combining temperature and air velocity measurements
150 inside an empty and loaded insulated box with PCM have been conducted.

151 The present study attempted to bridge this research gap. The objective was to investigate
152 experimentally the airflow and heat transfer due to natural convection in an insulated box with
153 PCM. The influence of the PCM position and that of the presence of a load on flow patterns
154 and temperature distribution in the insulated box were examined in the study. A non-intrusive
155 technique, Particle Image Velocimetry (PIV), was implemented to characterize the air velocity
156 field. The originality of this study lies in a) the implementation of PIV measurement for low air
157 velocity and b) the analysis of both velocity and temperature fields in different configurations
158 of an insulated box with PCM under a real use condition of food transport i.e., all walls of the
159 box subjected to heat losses and the presence of loads in the box. The obtained knowledge
160 would be useful to suggest the optimal practices for handling insulated boxes used for food
161 transport. The experimental results obtained in this study enable deep knowledge in the
162 exchange phenomena. They will be used to develop CFD and simplified thermal models, which
163 will be presented in the future. These numerical approaches enable the prediction of product
164 temperature change with time at different positions in an insulated box exposed to variable
165 ambient temperatures as in a real shipment.

166 **2. Materials and methods**

167 **2.1 Experimental device**

Two insulated boxes were used. Box A was a commercially manufactured box which was used for the thermal study (temperature measurement by thermocouples). Box B was the same box in which two walls were replaced with triple-glazed windows ensuring almost the same insulation, and it was used for the momentum study (air velocity measurement by a PIV system). As shown in **Fig. 1a**, the wall structure of Box A is composed of an expanded polystyrene foam layer (thickness: 25 mm, λ = 0.029 $W \cdot m^{-1} \cdot K^{-1}$) sandwiched between two polypropylene plastic layers (thickness: 3.5 mm, λ = 0.12 $W \cdot m^{-1} \cdot K^{-1}$, ε = 0.97) (Cengel and Ghajar, 2020). The inner gap between the polypropylene layers is 35 mm so that an air layer (thickness: 5 mm, λ = 0.025 $W \cdot m^{-1} \cdot K^{-1}$) is also present. The internal dimensions of the box were 310 mm (W) × 500 mm (L) × 300 mm (H), corresponding to about 0.05 m^3 in volume. Box B had the same dimensions and wall structure, but two vertical walls were replaced by triple-glazed windows. They were composed of three glass layers (λ = 1.4 $W \cdot m^{-1} \cdot K^{-1}$) each with a thickness of 4 mm and two 10-mm argon gaps (λ = 0.018 $W \cdot m^{-1} \cdot K^{-1}$), as shown in **Fig. 1b.** In addition, the panes were coated with a low-emissivity material (ε = 0.03, manufacture data) to avoid the transmission of infrared radiation. In this manner, the overall heat transfer coefficient of the glass wall was almost identical to that of the unmodified commercially manufactured box: $U_g \cong U_w$ = 0.9 $W \cdot m^{-2} \cdot K^{-1}$. This makes it possible to consider that heat losses occurring in Boxes A and B were almost the same; thus, the momentum results obtained experimentally from Box B can be compared with the thermal results obtained from Box A.

Tap water filled in a polypropylene recipient (280 mm × 460 mm × 50 mm) was used as a PCM for both thermal and momentum studies. The melting point and the latent heat of water is respectively -0.2°C (measured data) and 334 kJ/kg (Cengel and Ghajar, 2020) while the other thermophysical properties of water are given in **Table 1**. Although tap water was used, its properties are close to the ones of pure water since the amount of solute corresponding to the measured melting temperature (-0.2°C) is very low (around 0.05 mol/kg). The PCM was prepared (solidification) by placing horizontally in a freezer (-2.0°C set point) for at least 48 h before being used in each experiment to ensure that it was completely frozen at a temperature close to the melting point. Depending on the experimental conditions, the PCM was placed either on the top wall (lid) or on a vertical (side) wall of the box. (melting point of -0.2°C)

Two types of loads were used in the experiment: 4 inert blocks made of extruded polystyrene (XPS, dimensions 200 mm × 400 mm × 50 mm) and 16 packs of test product made of tylose (TYL, dimensions of a pack 200 mm × 100 mm × 50 mm). The presence of XPS blocks made it possible to study the influence of obstruction (without heat exchange with air) on the airflow pattern, while the presence of TYL packs made it possible to study the combined influence of obstruction and heat exchange with air. The use of XPS blocks made it possible to reach a thermal steady state (low thermal inertia) rapidly. Both types of loads were arranged so they had the same stack dimensions: 200 mm × 400 mm × 200 mm. The TYL packs were previously stored in a laboratory refrigerator and their initial core temperature was 5.0 ± 1.0°C before being used in the experiment. The 1.0°C temperature variation is related to the position of the pack in the refrigerator during preparation. It is to be emphasized that due to the large variety of food products and their thermophysical properties, the test product employed in the standard tests of refrigeration equipment was used. The properties of this test product (called Tylose) are close to those of meat product as shown in **Table 1**.

To facilitate interpretation of the results, the boxes (for both the thermal and momentum studies) were placed on small supports (with a height of 50 mm) placed on a table (with a height of 700 mm), thereby ensuring homogeneous airflow around the box (including underneath it). The experimental device was placed in a test chamber (dimensions: 340 cm × 340 cm × 250 cm) in which the ambient temperature was controlled at 20.0 ± 1.0°C throughout the experiments. The humidity in the room was not controlled. The relative humidity measured by using a hygrometer (Testo 174H, accuracy ±3%rh) lied in the range of 45-65%, corresponding to the humidity ratio of 0.006–0.009 kg of water vapor/kg dry air.

2.2 Thermal study

Temperature measurements were performed in Box A using calibrated T-type thermocouples (200 μm diameter, ± 0.2°C accuracy) connected to a data logger (Agilent 34972A). The protocols for the measurements under empty and loaded conditions are described hereafter.

2.2.1 Experimental protocol under empty conditions

The temperature measurements were conducted on a middle plane (x = 250 mm) of the box as shown in **Fig. 2a**. Twelve thermocouples were installed on a portable stand at intervals varying from 5 mm (near the top and bottom) to 35 mm (mid-height) and were used to measure the air temperatures across the cavity. Another twelve thermocouples were fixed on the surfaces of the box walls and the PCM in order to measure their surface temperatures. Three thermocouples were also installed at three positions inside the PCM.

To establish the temperature profiles, several temperature measurements were carried out by moving the stand from one position to another across the plane. The stand was positioned at a distance of 5 mm from the walls for the initial measurement. The measurement began at least 90 min. after the box closure (steady state had been reached) and lasted for a duration of 5 min. with recording intervals of 15 s. The box was re-opened in order to move the stand to the next position and then was closed rapidly to limit the effects of external air ingress (total duration of this operation: < 1 min). Then, temperature measurement was undertaken 15 min. after closure (steady state had been reached again). To address the temperature profile in the boundary layer, fine incremental steps of 5 mm were applied for the first five positions near the wall, then coarser incremental steps (up to 50 mm) were used (eighteen y-positions). The temperature at each position was averaged over 5 min. and the reported temperature profiles were based on these average values.

It needs to be emphasized that the phase change process of the PCM is a transient phenomenon and the real steady state never exists. The "pseudo" steady state stipulated in this study indicate

the duration in which the air temperatures at different positions in the cavity were relatively constant. Preliminary experiments showed that "pseudo" steady state was reached after 90 min. Then, the standard deviations over 3 h of the air temperatures at eight positions in the box never exceeded 0.3°C.

2.2.2 Experimental protocol under loaded conditions

The stack of TYL packs was carefully placed in the center of the box, which corresponded to a loading percentage (including the PCM) of almost 50% by volume. In this case, all air and load temperatures (core and surface) were simultaneously measured throughout the experiment without intermittent openings. **Fig. 2b** shows the positions of the thermocouples used to measure the air temperatures on the middle (x = 250 mm) and the lateral (x = 15 mm) planes of the box as well as the core and surface temperatures of four TYL packs. Thermocouples were also installed at three positions inside the PCM. Measurements were undertaken 90 min. after the closure of the box and lasted until the PCM was completely melted (i.e. all measured PCM temperatures started to increase). A recording interval of 30 s was set for the experiment. The air and product (core and surface) temperatures at each point were averaged over 200 min. during which the PCM was melting. These time-averaged values were used to establish the temperature field in the loaded box.

2.3 Momentum study

Fig. 3 shows the overall view of experimental setup for the air velocity measurements in the insulated box (Box B) using a PIV system which requires tracer particles (oil smoke in our case) for the measurement. The box was connected to a smoke container using a flexible duct in which four small PCM packs were used to precool the smoke before entering the box. A small fan was used to assist the introduction of precooled smoke (~10°C) into the box and its flow rate was controlled by a valve on the connecting duct.

2.3.1 PIV system

A 2D-PIV system (LaVision, FlowMaster 2D) was used to visualize the flow pattern and to measure air velocity in the box. The system is composed of three main components: a double-pulsed Nd:YLF laser (527 nm wavelength, 10 mJ pulse energy), a high-speed 12-bit CMOS video camera (Photron, FASTCAM SA3; 1024 ×1024 pixels in resolution) mounted with a lens (Sigma; 105 mm, f/1:2.8), and a programmable timing unit (PTU-X) for the synchronization of the device. For light scattering, a smoke machine (Antari, F-80Z) was used to generate oil particles (Levenly, Smoke Standard; mean diameter of 0.3 μm). Image acquisition and post-processing were performed using DaVis 10.2 interfaced software. The camera and the laser were installed on a three-dimensional displacement system (displacement precision ± 1 mm) and aligned in such a manner that the field of the camera view was perpendicular to the light sheet (thickness of 1 mm).

2.3.2 Image acquisition

The PIV measurements under both unloaded and loaded conditions were performed on the same plane as the temperature measurement under loaded conditions: the middle plane (x = 250 mm) and the lateral plane (x = 15 mm). Based on the image calibration using a ruler and the DaVis software, the magnification factor of 0.113 mm/pixel was determined and it corresponded to an image size of approximately 115 mm × 115 mm. For each measurement plane, several measured windows with a partial overlap between them were used to cover the entire area of the plane. **Fig. 4** shows the position and its corresponding number of measured windows on the measurement plane for different experimental conditions (unloaded/loaded and PCM on the side/lid). The position of the measured windows was changed by using a displacement system.

For each measured window, 500 pairs of images were recorded every 20 ms with a time interval (Δt) between two paired images (two pulsed laser illuminations) of 900 μs, and the total

measurement duration was 10 s. Based on the preliminary experiment, the measurement duration should not exceed 10 s to avoid heat generation by the laser which caused an increase in wall temperature, thereby affecting airflow. This time interval was considered as an optimal value for a velocity estimation in our case, because it allowed a mean particle displacement of less than a quarter of the smallest width of interrogation window (Keane and Adrian, 1992).

2.3.3 Image post-processing

A multi-pass correlation algorithm was used to process instantaneous vector calculation. The cross-correlation between individual paired images was performed with decreasing interrogation window sizes: 64 × 64 pixels with 50% overlap for the first passes and 32 × 32 pixels with 75% overlap for the final passes. Given the interrogation dimensions of the final pass, the spatial resolution of the vector field (distance between two vectors) was 8 pixels (about 0.9 mm) in both vertical and horizontal directions. After 500 instantaneous vector fields were obtained, the mean velocity field (v: 2D velocity magnitude) was then calculated as follows

$$v = \frac{1}{N}\sum_{i=1}^{N}\sqrt{v_{y,i}^2 + v_{z,i}^2} \quad (1)$$

where N is the total number of measured windows (N = 500 in our case), v_y and v_z are the horizontal and vertical velocity components expressed in $m \cdot s^{-1}$, respectively.

The mean velocity fields of all measured windows were then connected to establish the velocity field of the entire measurement plane. It should be emphasized that the out-of-plane regions and the regions near high reflection surfaces in the images (e.g. the surfaces of PCM, wall, and load) were deleted and excluded prior to the vector calculation.

The DaVis software uses the correlation statistics method (a-posteriori approach) to quantify the uncertainty of the PIV measurement. Based on the statistical analysis (Wieneke, 2015), the

uncertainty of the mean air velocity reported in this study was less than 5% for v > 0.04 m·s^{-1} and less than 10% for 0.02 < v < 0.04 m·s^{-1}.

2.3.4 Experimental protocol

Air velocity measurements were carried out under steady state conditions which were achieved 90 min. after the PCM was introduced into the box. At steady state, the precooled smoke was introduced into the box until its concentration was sufficient. To ensure flow stabilization, the PIV measurement was performed about 30 min. after the smoke introduction. Nine and five measured windows of 500 paired images were captured for the experiments under empty and loaded conditions, respectively. **Table 2** summarizes all experimental conditions for the temperature and the velocity measurements.

3. Results and discussion

3.1 Air velocity and temperature profiles under the empty condition

The experiment was firstly performed under empty conditions to gain an understanding of underlying momentum and energy transport phenomena inside the insulated box equipped with PCM. The influence of PCM positions (side wall and lid) on these phenomena were investigated and the results are presented as follows.

3.1.1 PCM on a side wall of the box

When the frozen PCM was placed on a side wall of the box, the apparent width (W') of the box was reduced to 260 mm and accordingly the aspect ratio ($A = H/W'$) of the box was about 1.15. Based on the temperature difference between the inner surfaces of the PCM and the walls ($\Delta T = T_h - T_c$ = 7.9°C), the Rayleigh (Ra) number based on the box height as defined in **Eq.**

2 was approximately 2.8×10^7. Thus, the air flow in the box was in the laminar regime ($< 10^9$) (Saury et al., 2011).

$$Ra = Gr \cdot Pr = \frac{g\beta(T_h - T_c)H^3}{\upsilon^2} \cdot \frac{c_p \mu}{\lambda} \qquad (2)$$

The thermal properties of air were calculated at the mean air temperature in the box (T_{mean} = 7.7°C) by using the correlations proposed by McQuillan et al. (1984). The calculated values are summarized in **Table 3**.

Fig. 5 shows the air velocity profiles on the middle (x = 250 mm) and the lateral (x = 15 mm) planes of the box equipped with the PCM on the side wall. For comparison purposes, the color scale was limited to 0.13 $m \cdot s^{-1}$ over which the maximum value recorded among all experimental conditions never exceeded. Large (red) arrows were drawn over the velocity field in order to provide better visualization of flow patterns represented by velocity vectors originally generated from the PIV software.

As shown in **Fig. 5a**, the airflow on the middle plane exhibits a flow pattern similar to the simple case, largely documented in the literature, of a rectangular cavity with opposite isothermally hot and cold vertical walls and well-insulated horizontal walls (Lee and Lin, 1995): upward and downward flow streams adjacent to the vertical surfaces of the side wall and the PCM, respectively. These flow streams moved horizontally along the bottom and the top walls, respectively, thus forming a recirculation cell. However, due to the technical limitations of the experimental device, the visible height was limited to z = 260 mm; thus, the complete flow recirculating cell could not be visualized in our study (dashed-line arrow in **Fig. 5a**).

A secondary flow was also detected (see arrow A on **Fig. 5a**): the air at a distance of about 30 mm from the box wall changes its direction from upward to downward and flows toward the cold wall. This could result from the heat transfer through the bottom wall of the box. The

airflow near the 'warm' bottom wall has a slightly ascending slope (this is not the case for an adiabatic bottom wall). The air located about 30 mm from the walls is entrained by the main recirculation flow, but it is relatively colder than the air nearer to the wall; thus, at a given point, its trajectory leaves the main cell and becomes downwards.

As illustrated in **Fig. 5a'**, the vertical velocity component (v_z) near the box wall tended to increase from bottom to mid-height (z = 120 mm) reaching almost 0.09 m·s^{-1}. Beyond this height (z > 120 mm), the velocity started to decease. A similar trend was observed near the PCM, but in the opposite manner. The vertical velocity component ($|v_z|$) steadily increased from the top until roughly z = 90 mm reaching almost 0.08 m·s^{-1}, then the velocity began to decrease, conceivably because the flow 'turned' at the corner. The flow pattern on the lateral plane (**Fig. 5b**) was almost identical to that on the middle plane, but the maximal velocity magnitude was higher (0.12 m·s^{-1}). Note that the velocity field on the lateral plane (x = 15 mm) was extended to the region of the PCM because the PCM was symmetrically placed in the box, thereby allowing the PIV measurement in the gap between the lateral wall and the PCM (x > 20 mm).

On both planes, there is a zone of stagnant air in the core region of the box. However, this region on the lateral plane was smaller than that on the middle plane. Three-dimensional flow due to additional heat gain through the side wall could explain this difference.

Fig. 6a shows the air temperature field on the middle plane (x = 250 mm) of the box with PCM on the side wall. This temperature field was plotted by interpolation from 252 measurement points over this plane by using MATLAB. The temperature field shows the thermal boundary layers. Due to heat conduction from the exterior, the air temperature increases constantly while it flows along the box walls, and the boundary layer thickness increases. Then, the air is cooled down along the PCM. This is coherent with the flow pattern (recirculation cell) observed by the

PIV measurement. Overall stratification was observed: colder air near the bottom, and warmer air near the top. The maximum air temperature was about 10°C at the top corner on the side wall and the minimum air temperature was observed at the bottom corner on the PCM side. The surface temperature of the PCM container varied from 0.5°C at the bottom (z = 20 mm) to around 3.5°C at the top (z = 230 mm). Thermal boundary layers at different heights are illustrated in **Fig. 6b**. As expected, their thickness was close to hydrodynamic thicknesses **(Fig. 5a')** since the Prandtl number is relatively close to 1 (Pr = 0.71).

3.1.2 PCM on the lid of the box

The apparent height was H' = 250 mm; thus, the aspect ratio of the box with PCM on the lid ($A = H'/W$) was about 0.81 and the Ra number was 2.4×10^7 (ΔT = 6.8°C). As in the case of PCM on the side wall, the airflow was laminar. The values of thermal properties of air are summarized in **Table 3** (T_{mean} = 6.2°C).

Fig. 7 shows the air velocity profiles on the middle (x = 250 mm) and the lateral (x = 15 mm) planes of the box with PCM on the lid. It was found from **Fig. 7a** that there were two almost symmetric, counterrotating air-flow cells. This result qualitatively agrees with the numerical solution obtained by Corcione (2003) who also observed such a two-cell flow pattern in a rectangular cavity with one cold top wall, one hot bottom wall and two hot side walls (A = 0.5 and Ra = 10^6 in his study). As shown in **Fig. 7a'**, the positive vertical velocity components were detected along the side walls (y < 50 mm and y > 260 mm) while the negative ones were mostly in the core region. On the middle plane, the absolute values of the vertical velocity components never exceeded 0.08 $m\cdot s^{-1}$. The upward flow along the side walls was induced by the relatively high air temperature in these regions as a result of heat conduction through the box walls. Accordingly, these flow streams converged on the top where air was cooled down via the PCM. Becoming heavier, the air then flowed downward in the center region.

Near the lateral wall (x = 15 mm, **Fig. 7b and b'**), the flow is almost everywhere upwards as is the case near the side wall (v_z > 0 for y = 15 mm in **Fig. 7a'**). In fact, one would expect a similar 2D cell flow pattern in x-z plane ($y = W/2$) as that observed in the y-z plane ($x = L/2$, **Fig. 7a**). Overall, air flows upwards along the lateral and side walls, whereas it flows downward in the central region (3D flow). Near the corners (junction of lateral and side walls e.g. x = 15 mm, y = 15 mm) the heat flow by conduction through the walls is the highest, and this explains why the vertical velocity is also the highest in these positions: 0.12 $m \cdot s^{-1}$.

It should be borne in mind that the presented velocity fields are time-averaged over 10 s and are composed of 9 windows recorded at different times (typically at 2 min. intervals taking into account the time needed to move the camera and save the recorded data). Direct observation of smoke in the middle plane showed that the flow was not stable (it was unsteady) in the central region: the downward flow oscillated in the y direction. This explains why the velocity observed in **Fig. 7a** is not strictly symmetric and that there are some 'jumps' between the 3 parts (3 windows in the y direction) of the profiles in **Fig. 7a'**. This type of instability has been observed also for free convection in domestic refrigerators (Laguerre et al., 2005).

Fig. 8 shows the air temperature field on the middle plane of the box. As expected, the cold region was in the center where downward flow was observed, while the warm region was near the side walls where upward flow was observed. The maximum air temperature was about 9°C near the top of the side walls and the minimum air temperature was observed just below the PCM (top of central region); the surface of the PCM container was at a temperature of around 1-2°C.

3.1.3 Comparison between PCM on the lid or on the side

In comparison with the case of PCM on the side wall, the box with PCM on the lid exhibited a lower maximal temperature: 9.3°C (lid)/10.5°C (side). This high temperature was observed near

the walls. In fact, the product should not touch the walls and should even be placed outside the boundary layers whose thickness was around 30 mm. If we exclude the boundary layer zone, the mean temperature (in the middle plane) was lower for PCM on the lid: T_{mean} = 6.2°C (lid) and 7.7°C (side) and the temperature distribution was also more homogeneous for PCM on the lid: $T_{max} - T_{min} = 1.7$°C (lid) and 2.7°C (side).

As mentioned previously, flow fluctuations were visually observed in the central region where the PCM was placed on the lid. To a lesser extent, fluctuations were also observed near the bottom of the PCM when it was placed on the (right) side. **Fig. 9** presents the instantaneous velocity evolution during 10 s at two positions (near the center and near the bottom/right corner). This confirms that the airflow was more stable in the case of PCM on the side. Velocity variations of up to 0.10 m·s^{-1} were detected at the center of the box with PCM on the lid (**Fig. 9b**).

The convective heat transfer coefficients can be estimated from the measured temperature profiles. Very near to the wall, the air velocity is close to zero. So, the heat flux (W·m^{-2}) along y-direction can be given by

$$\lambda_a \frac{\partial T}{\partial y} = h_z(T_w - T_\infty) \qquad (3)$$

where T_w and T_∞ are the temperatures of the wall and the air outside the boundary layer (free stream), respectively, λ_a is the thermal conductivity of the air, and h_z is the local convective heat transfer coefficient at a given height (z) which can be approximately estimated from

$$h_z = \frac{\lambda_a(\partial T/\partial y)}{T_w - T_\infty} \qquad (4)$$

For example, when the PCM was at the side wall, at the mid height (z = 160 mm), the temperature at the PCM wall, at 5 mm from the wall and outside the boundary layer were 0.8°C, 5.5°C and 7.2°C, respectively. The slopes ($\partial T/\partial y$) of the tangent line to the temperature profile near the PCM wall was thus approximately 1°C/mm. Accordingly, the local convective heat transfer coefficient at PCM wall could be estimated around 4 W·m^{-2}·K^{-1}. In the same way, the

heat transfer coefficient at the vertical internal box walls (warm walls) could be estimated between 2 and 3 $W \cdot m^{-2} \cdot K^{-1}$. It is to emphasize that the temperature fields were measured only during the 'pseudo' steady state period during which the air temperature was almost invariant with time. Therefore, the estimation of h_z was given for this period only.

Despite low heat transfer coefficients, convection cannot be neglected compared to conduction in air because the maximum air velocities observed in the box were around 0.1 $m \cdot s^{-1}$, corresponding to the Peclet number (Pe) of more than 100.

The Peclet number (Pe) is defined as

$$Pe = \frac{v_a L_c}{\alpha_a} \qquad (5)$$

For the empty box, the value was approximately 1500, given that the characteristic length (L_c) was 0.3 m (height of the box), the air velocity (v_a) was 0.1 $m \cdot s^{-1}$, and the air thermal diffusivity (α_a) was about 2×10^{-5} $m^2 \cdot s^{-1}$.

3.2 Air velocity and temperature profiles under loaded conditions

The experiments were performed under loaded conditions. The experiment was firstly conducted with inert blocks (XPS) that made it possible to study the obstacle-effect alone on the flow pattern. Then, an experiment with the test packs (TYL) was performed to study both the obstacle-effect and the influence of heat exchange with air. Due to the presence of the obstacles, the light sheet was restricted; thus, the velocity field behind the load was not available.

3.2.1 PCM on the side wall of the box

As shown in **Fig. 10**, the airflow in the loaded box, regardless of obstacle types, exhibited similarities with that in the empty box: upward and downward flow streams close to the vertical

surfaces of the side wall and the PCM, respectively. However, under loaded conditions, the upward flow on the middle plane did not result from a two-dimensional recirculation cell (located in this plane) but instead from a three-dimensional flow pattern as illustrated in **Fig. 11**. At State 1, the air flowed downward (-z direction) in the space between the PCM and the load. Once approaching the bottom wall (State 2), the air flowed rather horizontally (+/- x direction) toward the lateral walls of the box. At the edge of the load (State 3), the air turned and flowed between the lateral wall and the load (-y direction). This is confirmed in **Figs. 10b** and **10d** (lateral plane, x = 15 mm) where a strong flow from the right to the left was observed in the bottom region. When it reached the bottom of the side wall (State 4), the air moved both horizontally to occupy the entire gap between the side wall and the load and upwards because it became warmer and warmer (heat exchange with the walls). Finally, starting from State 5, it recirculated to the PCM.

The velocity fields obtained with inert blocks (XPS) and with test products (TYL) were very similar. This is because thermal steady state was practically reached in both cases (the test products were introduced practically at the equilibrium temperature and the measurement began after 2 h). In this manner, thermal inertia became negligible. For XPS (with very low thermal conductivity) the air temperature was expected to be relatively homogeneous in the gaps between the load and the lateral wall or the PCM. For TYL, due to conduction, the load surface temperature was lower than the air temperature in the wall-side gap but higher in the PCM-side gap (as shown hereafter in **Fig. 12a**). This could diminish free convection, but the results showed a minor effect (Pe ~150, L_c (gap) = 30 mm). This means that (steady state) flow characterization can be carried out with inert blocks (XPS), which is much simpler. Certainly, if warm products were introduced in the box initially, the flow pattern would have been substantially altered.

Fig. 12 shows the temperature field on the middle (x = 250 mm) and the lateral (x = 15 mm) planes of the box with PCM on the side wall and TYL load. The temperature field was coherent with the flow pattern: air was cooled down along the PCM and warmed up along all the box walls. It is obvious that the cold air near the PCM resulted in relatively low load temperatures on this (right) side. Conversely, the warmer air near the wall resulted in relatively high load temperatures on the opposite (left) side. Conduction in the load was not sufficient to homogenize the load temperature. The highest load temperature, 7.8°C, was reached near the side wall (opposite the PCM location). The average load temperature was 6.0°C and the maximum difference was 3.9°C. Air temperature stratification was observed on the lateral plane of the box (**Fig. 12b**).

3.2.2 PCM on the lid of the box

A complex flow pattern was observed in the loaded box with PCM on the lid as shown in **Fig. 13**. On the middle plane (x = 250 mm, **Figs. 13a** and **13c**), regardless of load types, cold air coming from the top (near the PCM) flowed downward in the center of the (left) gap between the side wall and the load. Then, air flowed upwards along the side wall and the load surface. An explanation for the upward flow along the side wall is that the air near this wall is warmed up by conduction through the wall (as in the empty case). The flow direction along the load surface is logically upwards if the surface temperature is higher than the average air temperature in the gap. This was the case for the XPS load because radiation from the wall to the load surface tended to increase the load surface temperature. For the TYL, in addition to radiation, conduction also occurred inside the load. This could explain why upward flow occurred all along the XPS load but occurred only along the upper part of the TYL load. This difference appeared also on the lateral plane (x = 15 mm): there were more upward flow regions in the

524 case of the XPS load. However, the easier experiments with the XPS load gave a good
525 approximation of the flow pattern in the presence of load in the box.

526 Due to the limitations of the PIV technique, velocity measurement was not possible in the (right)
527 gap. A similar flow pattern could be expected due to symmetry. However, in fact, flow was not
528 symmetrical above the load: it seemed that a stronger cold air stream flowed down in the right
529 gap than in the left gap. Such dissymmetry was already observed in the empty case (PCM on
530 the lid) where instability was induced by oscillations of downward flow. It seemed that in the
531 loaded case, the flow 'chose' one or another preferential pathway (through the left or right gap).
532 This is related to the non-linear term in the flow equations (Navier-Stokes) which is responsible
533 for a break in symmetry (even before turbulence). This dissymmetry was also confirmed by
534 **Figs. 13b** and **13d** (lateral plane, x =15 mm) where flow from the right to the left was observed
535 in the lower part of the box. The small difference in heat transfer coefficient between the left
536 (insulated wall) and the right (triple-glazed windows) can also induce dissymmetry.

537 **Fig. 14** presents the temperature field on the middle (x = 250 mm) and the lateral (x = 15 mm)
538 planes of the box with PCM on the lid and TYL load. It shows the thermal boundary layers
539 along the side wall (which explains upward flow along the walls). However, the load surface
540 temperature seemed very close to the adjacent air temperature. At the center of the gap (where
541 downward flow was observed) the air rapidly warmed up (the temperature was well above the
542 PCM surface temperature). This can explain the weak velocity observed in the gap.
543 Dissymmetry was also observed: the right gap had a lower average air temperature than the left
544 gap which in turn affected the load temperature. This also seemed to be due to a stronger cold
545 air stream from the PCM toward the right gap (see the red arrow in **Fig. 14**). For temperature
546 measurements, the dissymmetry cannot be imputed to a difference in insulation (Box A was

used). This configuration did not allow stratification since the cold PCM container was placed at the top.

In the case of PCM on the lid, the highest load temperature, 7.3°C (7.8°C for PCM on the side) was reached near the bottom (opposite the PCM location). The average load temperature was 5.7°C (6.0°C for PCM on the side), and the maximum difference was 3.0°C (3.9°C for PCM on the side). So, there was little apparent difference between the two configurations. These findings suggested that the PCM can be placed either at the side wall or at the lid without compromising the quality and safety of food products if spaces between the PCM and the load and between the side walls and the load are reserved. According to our estimation, the insulated box with ice as a PCM is feasible for the transport of food products in the temperature range of 4-8°C for about 10 h. The experimental results obtained by this study will be used for the development of CFD and simplified thermal models to predict product temperature evolution along a logistic chain. This evolution makes possible the prediction of product quality thanks to a relation with the product temperature. In this manner, the product shelf life under different logistic scenarios can be predicted. The thermal and quality modelling would help the supply chain management to optimize the logistic conditions to reduce food loss and waste.

4. Conclusions

The present study was carried out to characterize the airflow and the heat transfer due to natural convection in an insulated box equipped with PCM by using PIV technique and temperature measurement. The influence of the PCM position on the flow pattern and temperature distribution was investigated. The study was conducted in a progressively more complex manner: empty, loaded with extruded polystyrene (low conductivity and almost no thermal inertia), and loaded with tylose (thermal properties close to those of food). The key findings are summarized as follows:

Whatever the configuration, the highest observed air velocities were around 0.1 $m \cdot s^{-1}$; therefore, convection cannot be neglected compared to conduction in air (Peclet number > 100). Numerical simulations with either CFD or simplified models should include free convection.

When the PCM is on the side wall, the flow pattern is simple to predict. Air flows downwards along the PCM surface and upwards along the side walls. In the empty case, the flow pattern can be approximated by a 2D recirculation cell, but the presence of the load leads to a 3D flow pattern. When the PCM is on the lid, after cooling down in contact with the PCM, a cold air stream detaches from the PCM surface and flows downwards. This cold air stream is unstable in the empty case and shows preferential pathways (symmetry breaking) in the loaded case. The flow pattern is less predictable.

In all cases, after cooling down near the PCM, the air temperature increases progressively along the trajectories until returning close to the PCM. The product surface temperatures are close to the temperature of the adjacent air. At steady state, conduction in the load has a minor effect on the flow pattern which can be approximated by replacing the real load with an obstacle of low conductivity.

From a practical point of view, it is recommended to leave a space between the PCM and the load (to promote free convection) and between the side walls and the load (to allow evacuation of heat from the ambient via conduction through the walls). The gap should be at least of the order of the boundary layer thicknesses: 2-3 cm. Further experiments without such gaps would be useful.

At thermal steady state, there was no significant difference in terms of maximum product temperature and heterogeneity between the PCM on the lid or at the side. The study showed the coldest and warmest zones in both cases, suggesting the best location for products that are sensitive to bacterial growth or chilling injury.

Further studies are planned in order to compare these results with CFD simulations and to develop a simplified model that enables prediction of temperature evolution (at different locations) as a function of the box, the product and PCM properties, along with ambient temperature changes.

Acknowledgements

The authors gratefully acknowledge King Mongkut's Institute of Technology Ladkrabang, Thailand (contract no. KREF156402), the French Embassy in Thailand, and the National Research Institute for Agriculture, Food and Environment, France, for their financial support. The first author, T. Leungtongkum, would also like to thank the Office of the Civil Service Commission of Thailand and Chulalongkorn University, Thailand, for the awarding of his PhD scholarship. The authors thank to LaVision for PIV technical support.

References

Aitlahbib, F., & Chehouani, H. (2015). Numerical study of heat transfer inside a Keeping Warm System (KWS) incorporating phase change material. *Applied Thermal Engineering* 75, 73-85.

Ataei-Dadavi, I., Chakkingal, M., Kenjeres, S., Kleijn, C.R., & Tummers, M.J. (2019). Flow and heat transfer measurements in natural convection in coarse-grained porous media. *International Journal of Heat and Mass Transfer* 130, 575-584.

Bergman, T.L., Incropera, F.P., DeWitt, D.P., & Lavine, A.S. (2011). *Fundamentals of heat and mass transfer*. John Wiley & Sons.

Çengel, Y.A., & Ghajar, A.J. (2020). *Heat and mass transfer : fundamentals and applications*. Mcgraw-Hill Education, New York, NY.

Choi, S.J., & Burgess, G. (2007). Practical mathematical model to predict the performance of insulating packages. *Packaging Technology and Science: An International Journal* 20(6), 369-380.

Corcione, M. (2003). Effects of the thermal boundary conditions at the sidewalls upon natural convection in rectangular enclosures heated from below and cooled from above. *International Journal of Thermal Sciences* 42(2), 199-208.

Du, J., Nie, B., Zhang, Y., Du, Z., & Ding, Y. (2020). Cooling performance of a thermal energy storage-based portable box for cold chain applications. *Journal of Energy Storage* 28, 101238.

East, A., Smale, N., & Kang, S. (2009). A method for quantitative risk assessment of temperature control in insulated boxes. *International journal of refrigeration* 32(6), 1505-1513.

Icier, F., & Ilicali, C. (2005). The use of tylose as a food analog in ohmic heating studies. *Journal of Food Engineering* 69(1), 67-77.

631 Jevnikar, S., & Siddiqui, K. (2019). Investigation of the influence of heat source orientation on
632 the transient flow behavior during PCM melting using particle image velocimetry. *Journal*
633 *of Energy Storage* 25, 100825.
634 Keane, R.D., & Adrian, R.J. (1992). Theory of cross-correlation analysis of PIV images. *Applied*
635 *scientific research* 49(3), 191-215.
636 Labihi, A., Aitlahbib, F., Chehouani, H., Benhamou, B., Ouikhalfan, M., Croitoru, C., & Nastase,
637 I. (2017). Effect of phase change material wall on natural convection heat transfer inside
638 an air filled enclosure. *Applied Thermal Engineering* 126, 305-314.
639 Laguerre, O., Aissa, M.B., & Flick, D. (2008a). Methodology of temperature prediction in an
640 insulated container equipped with PCM. *International journal of refrigeration* 31(6), 1063-
641 1072.
642 Laguerre, O., Amara, S.B., Charrier-Mojtabi, M.-C., Lartigue, B., & Flick, D. (2008b).
643 Experimental study of air flow by natural convection in a closed cavity: Application in a
644 domestic refrigerator. *Journal of Food Engineering* 85(4), 547-560.
645 Laguerre, O., Amara, S.B., & Flick, D. (2005). Experimental study of heat transfer by natural
646 convection in a closed cavity: application in a domestic refrigerator. *Journal of Food*
647 *Engineering* 70(4), 523-537.
648 Laguerre, O., Chaomuang, N., Derens, E., & Flick, D. (2019). How to predict product
649 temperature changes during transport in an insulated box equipped with an ice pack:
650 Experimental versus 1-D and 3-D modelling approaches. *International journal of*
651 *refrigeration* 100, 196-207.
652 Laguerre, O., Derens, E., & Flick, D. (2018). Modelling of fish refrigeration using flake ice.
653 *International journal of refrigeration* 85, 97-108.
654 Laguerre, O., & Flick, D. (2010). Temperature prediction in domestic refrigerators:
655 Deterministic and stochastic approaches. *International journal of refrigeration* 33(1), 41-
656 51.
657 Lee, S.H., Seo, Y.M., Yoon, H.S., & Ha, M.Y. (2016). Three-dimensional natural convection
658 around an inner circular cylinder located in a cubic enclosure with sinusoidal thermal
659 boundary condition. *International Journal of Heat and Mass Transfer* 101, 807-823.
660 Lee, T., & Lin, T. (1995). Three-dimensional natural convection of air in an inclined cubic cavity.
661 *Numerical Heat Transfer, Part A: Applications* 27(6), 681-703.
662 Leungtongkum, T., Flick, D., Hoang, H.M., Steven, D., Delahaye, A., & Laguerre, O. (2021).
663 Insulated box and refrigerated equipment with PCM for food preservation: State of the
664 art. *Journal of Food Engineering*, 110874.
665 Margeirsson, B., Palsson, H., Popov, V., Gospavic, R., Arason, S., Sveinsdóttir, K., & Þór
666 Jónsson, M. (2012). Numerical modelling of temperature fluctuations in superchilled fish
667 loins packaged in expanded polystyrene and stored at dynamic temperature conditions.
668 *International journal of refrigeration* 35(5), 1318-1326.
669 McQuillan, F., Culham, J., & Yovanovich, M. (1984). Properties of dry air at one atmosphere,
670 Microelectronics Heat Transfer Lab. *Rept. UW/M HTL* 8406.
671 Miroshnichenko, I., & Sheremet, M. (2018). Turbulent natural convection heat transfer in
672 rectangular enclosures using experimental and numerical approaches: A review.
673 *Renewable and Sustainable Energy Reviews* 82, 40-59.
674 Moreno, S., Hinojosa, J., Hernández-López, I., & Xaman, J. (2020). Numerical and
675 experimental study of heat transfer in a cubic cavity with a PCM in a vertical heated wall.
676 *Applied Thermal Engineering* 178, 115647.
677 Navaranjan, N., Fletcher, G.C., Summers, G., Parr, R., & Anderson, R. (2013). Thermal
678 insulation requirements and new cardboard packaging for chilled seafood exports.
679 *Journal of Food Engineering* 119(3), 395-403.
680 Orozco, D., Hinojosa, J., & Amaya, K. (2021). The effect of a segmented wall filled with Phase
681 Change Material on heat transfer and airflow in a closed cavity. *Journal of Heat Transfer*
682 143(9).
683 Pandey, S., Park, Y.G., & Ha, M.Y. (2019). An exhaustive review of studies on natural
684 convection in enclosures with and without internal bodies of various shapes. *International*
685 *Journal of Heat and Mass Transfer* 138, 762-795.

686 Paquette, J.-C., Mercier, S., Marcos, B., & Morasse, S. (2017). Modeling the thermal
687 performance of a multilayer box for the transportation of perishable food. *Food and*
688 *Bioproducts Processing* 105, 77-85.
689 Robertson, J., Franzel, L., & Maire, D. (2017). Innovations in cold chain equipment for
690 immunization supply chains. *Vaccine* 35(17), 2252-2259.
691 Saury, D., Rouger, N., Djanna, F., & Penot, F. (2011). Natural convection in an air-filled cavity:
692 Experimental results at large Rayleigh numbers. *International Communications in Heat*
693 *and Mass Transfer* 38(6), 679-687.
694 Singh, S., Burgess, G., & Singh, J. (2008). Performance comparison of thermal insulated
695 packaging boxes, bags and refrigerants for single-parcel shipments. *Packaging*
696 *Technology and Science: An International Journal* 21(1), 25-35.
697 Wieneke, B. (2015). PIV uncertainty quantification from correlation statistics. *Measurement*
698 *Science and Technology* 26(7), 074002.
699 Xiaofeng, X., & Xuelai, Z. (2021). Simulation and experimental investigation of a multi-
700 temperature insulation box with phase change materials for cold storage. *Journal of Food*
701 *Engineering* 292, 110286.
702 Zhao, X., Xia, M., Wei, X., Xu, C., Luo, Z., & Mao, L. (2019). Consolidated cold and modified
703 atmosphere package system for fresh strawberry supply chains. *LWT* 109, 207-215.
704 Zhao, Y., Zhang, X., & Xu, X. (2020). Application and research progress of cold storage
705 technology in cold chain transportation and distribution. *Journal of Thermal Analysis and*
706 *Calorimetry* 139(2), 1419-1434.

Table 1 Thermophysical properties of materials used in the study

Material	**Density [kg·m^{-3}]**	**Specific heat [J·kg^{-1}·°C^{-1}]**	**Thermal conductivity [W·m^{-1}·K^{-1}]**	**Reference**
Extruded polystyrene	35	1210	0.029	Cengel and Ghajar (2020)
Polypropylene	910	1925	0.120	Cengel and Ghajar (2020)
Tylose	1070	3372	0.510	Icier and Ilicali (2005)
Water (liquid)	1000	4217	0.561	Cengel and Ghajar (2020)
Water (solid)	920	2040	1.880	Cengel and Ghajar (2020)

Table 2 Experimental conditions for thermal (temperature measurement) and momentum (air velocity measurement) studies.

Conditions	**PCM position**	**Temperature measurement**	**Numbers of windows for air velocity measurement [window number]**	
			Middle plane	**Lateral plane**
Unloaded	Side wall	Yes	9 [1-9]	9 [1-9]
	Lid	Yes	9 [1-9]	9 [1-9]
Loaded (XPS)	Side wall	No	5 [1-5]	9 [1-9]
	Lid	No	5 [1-5]	9 [1-9]
Loaded (TYL)	Side wall	Yes	5 [1-5]	9 [1-9]
	Lid	Yes	5 [1-5]	9 [1-9]

XPS is a stack of four extruded polystyrene blocks (block dimensions = 200 mm × 400 mm × 50 mm); TYL is a stack of 16 Tylose packs (pack dimensions = 200 mm × 100 mm × 50 mm); the window number is referred to that in **Fig. 4**.

Table 3 Thermophysical properties* of air used for the Ra estimation.

Parameter	Unit	Value	
		T_a = 6.2°C	T_a = 7.7°C
ρ	kg·m^{-3}	1.264	1.258
υ	m^2·s^{-1}	1.387×10^{-5}	1.400×10^{-5}
c_p	J·kg^{-1}·°C^{-1}	1006	1006
λ	W·m^{-1}·K^{-1}	0.0245	0.0247
β	K^{-1}	0.0036	0.0036
*calculated at the average air temperature (T_a) from the correlations proposed by McQuillan et al. (1984)			

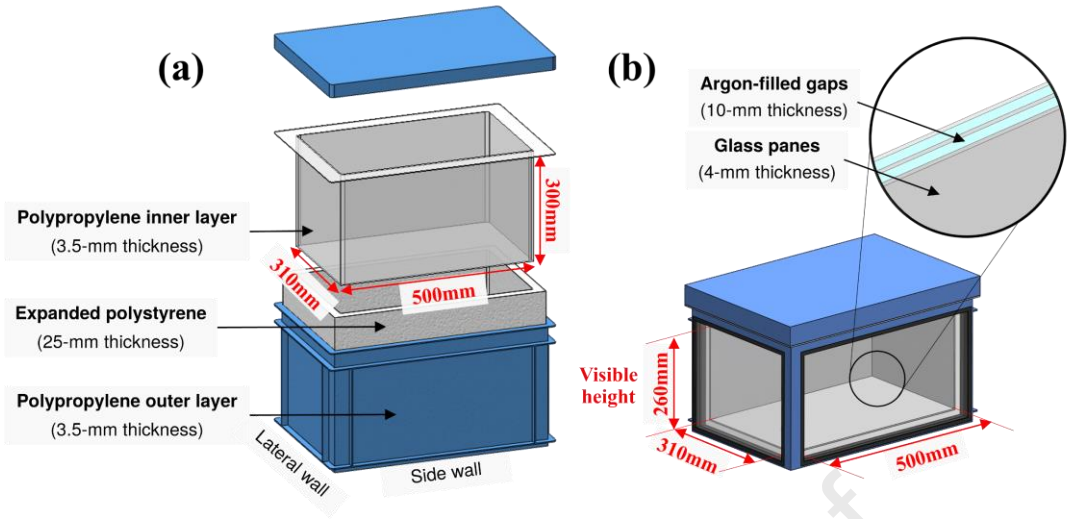

Fig. 1 Insulated boxes: (a) commercially manufactured box for temperature measurement (Box A); and (b) box with two walls replaced with triple-glazed windows for velocity measurement (Box B).

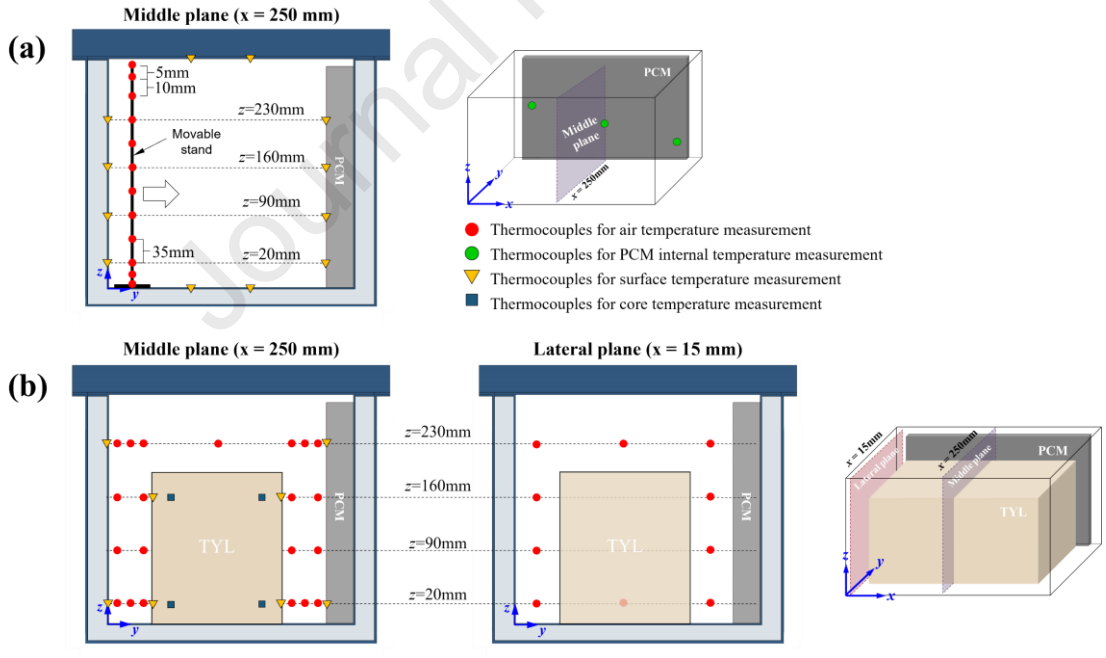

Fig. 2 Diagram showing the experimental setup for temperature measurement for PCM located on the side wall of (a) empty box, and (b) loaded box. TYL = Tylose packages.

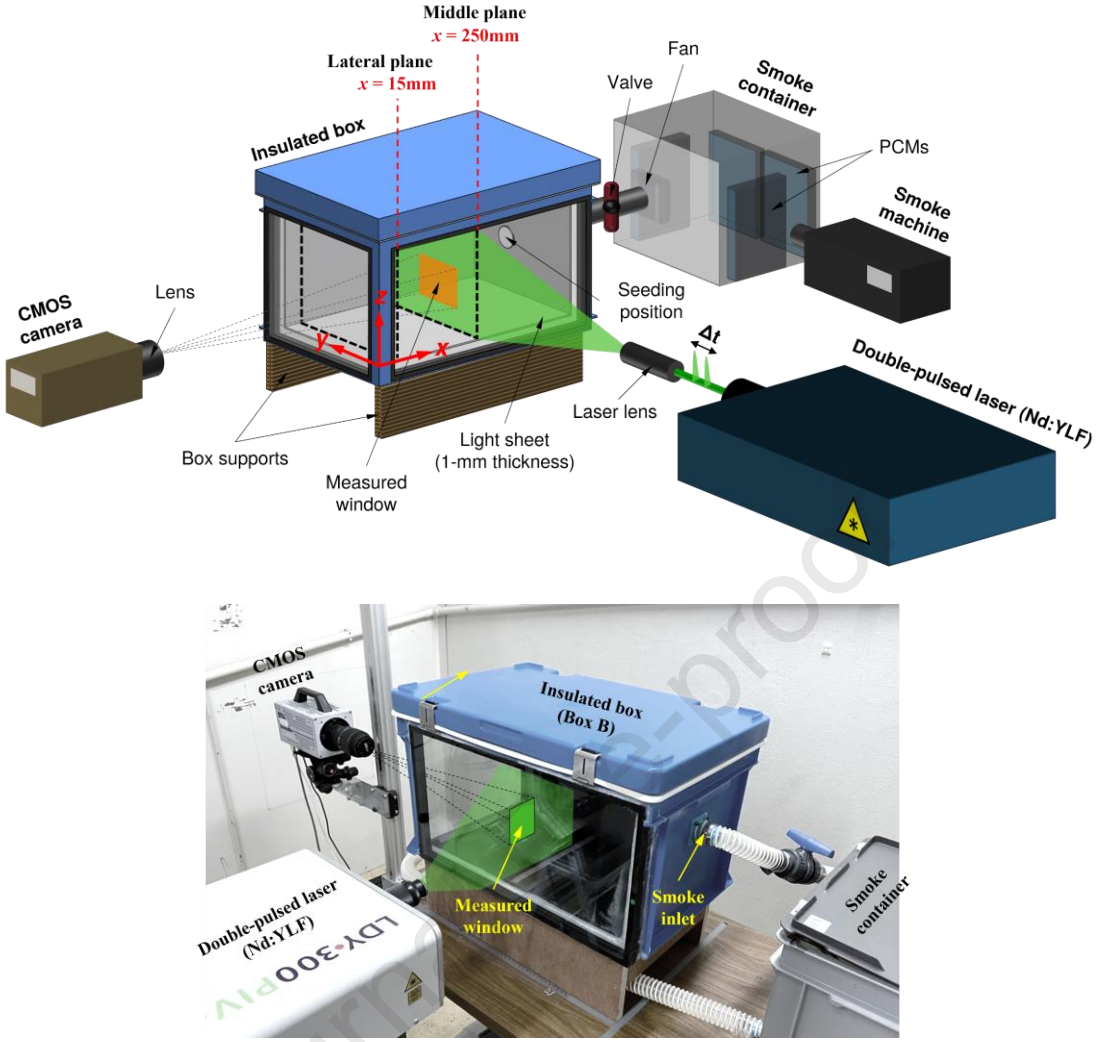

Fig. 3 Diagram (a) and photograph (b) showing the PIV setup.

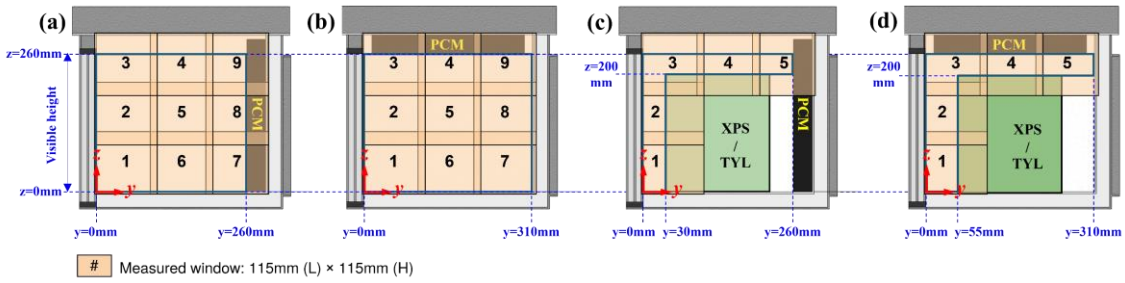

Fig. 4 Position of measured windows for the PIV measurement: (a) empty box/PCM on the side wall, (b) empty box/PCM on the lid, (c) loaded box/PCM on the side wall, and (d) loaded box/PCM on the lid.

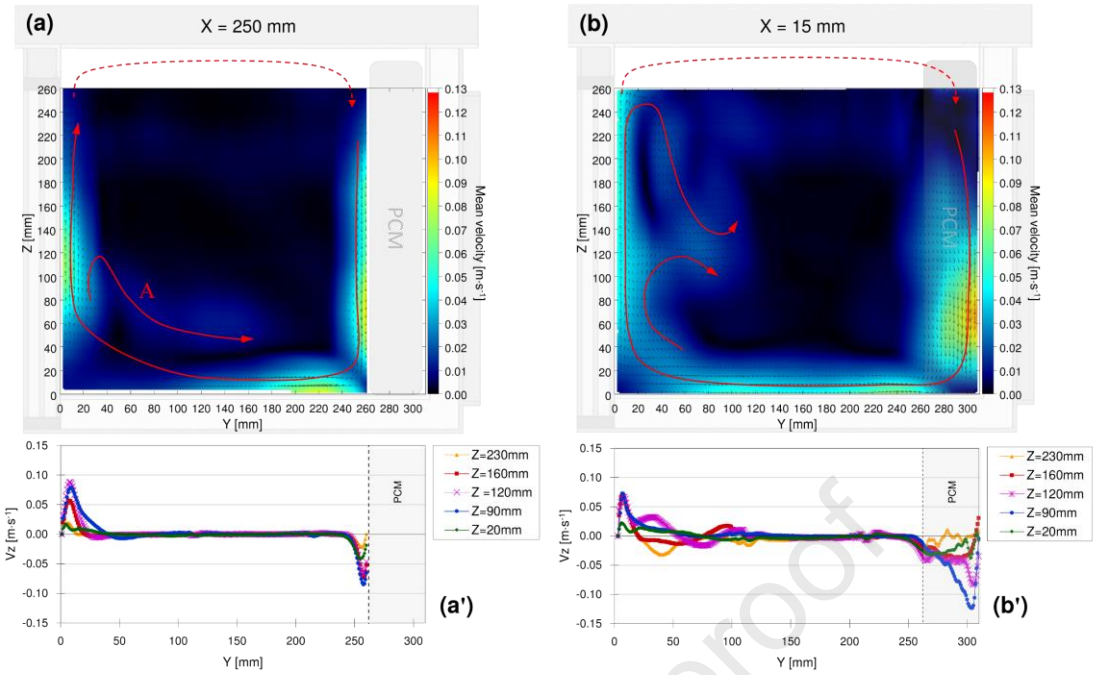

Fig. 5 Air velocity fields on (a) the middle (x = 250 mm) and (b) the lateral (x = 15 mm) planes of the box with PCM on the side wall. (a') and (b') are the profiles of the vertical velocity component (v_z) at 4 heights on the middle and the lateral planes, respectively.

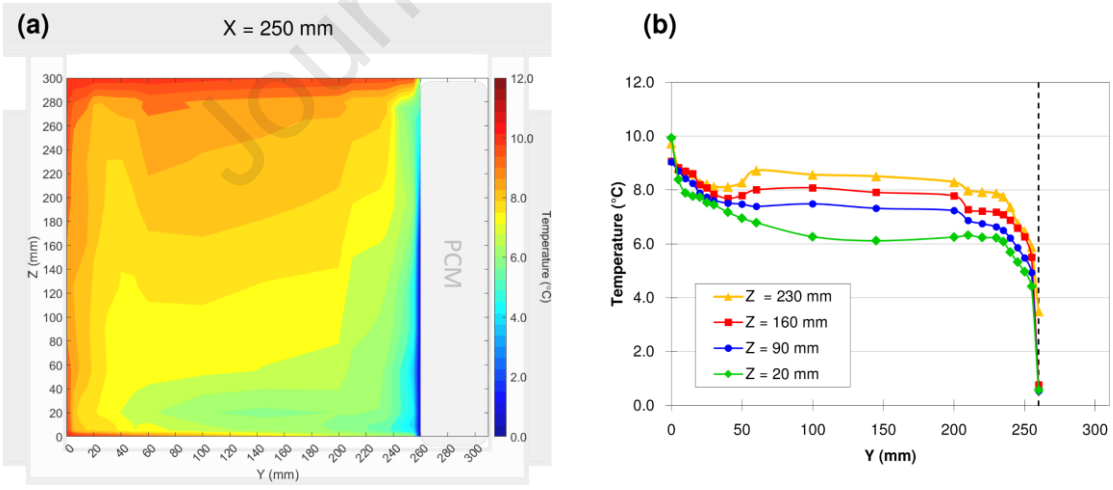

Fig. 6 (a) Air temperature field on the middle plane (x = 250 mm) of the box with PCM on the side wall and (b) temperature profiles at four different heights.

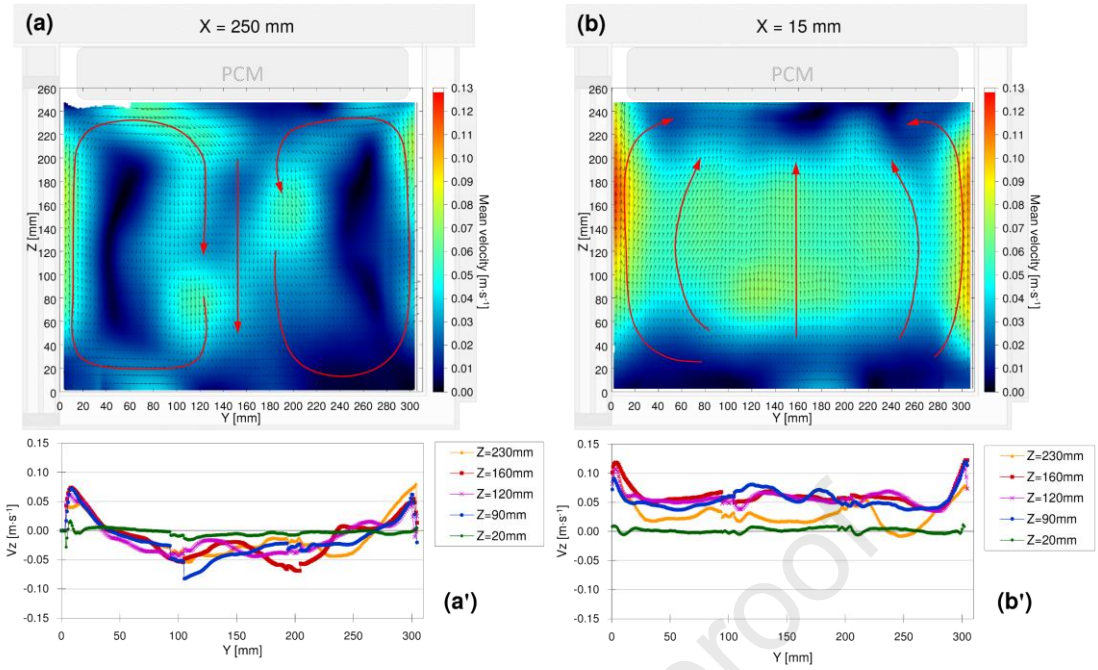

Fig. 7 Air velocity fields at (a) the middle (x = 250 mm) and (b) the lateral (x = 25 mm) planes of the box equipped with PCM on the lid. The profiles of the z-component of the velocity at 4 heights on (a') the middle and (b') the lateral planes.

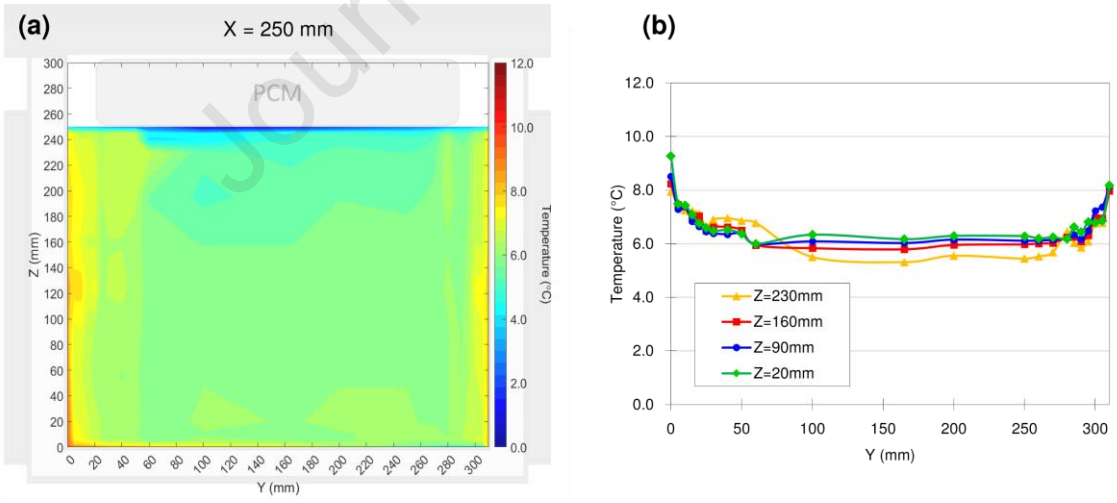

Fig. 8 Air temperature field on the middle plane (x = 250 mm) of the box with PCM on the lid.

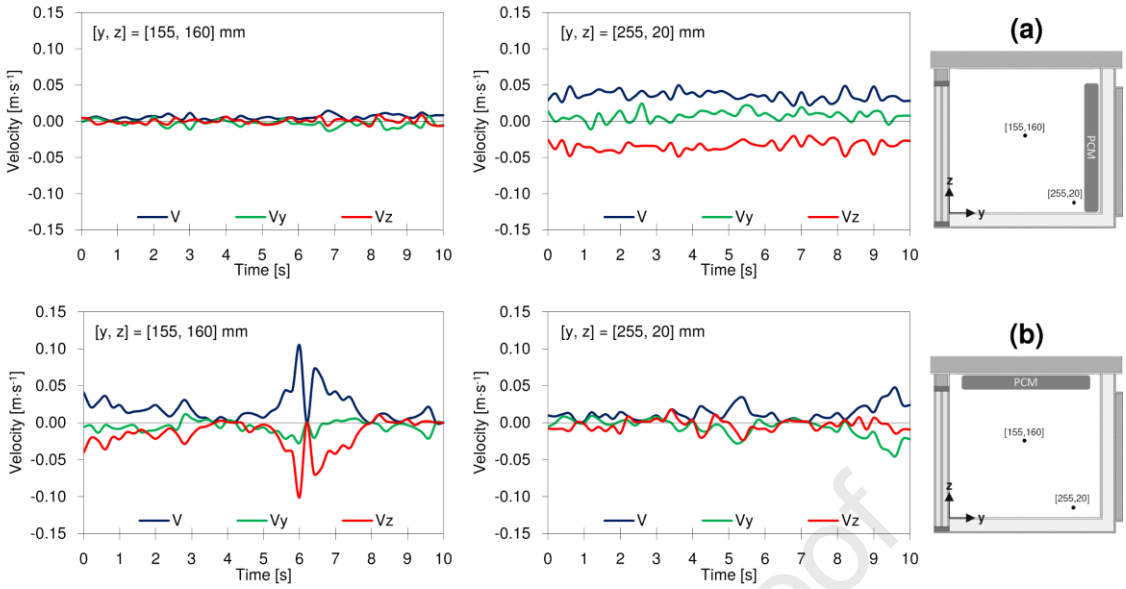

Fig. 9 Velocity variations of the air at the same two positions in the box with PCM on (a) the side wall and (b) the lid**.**

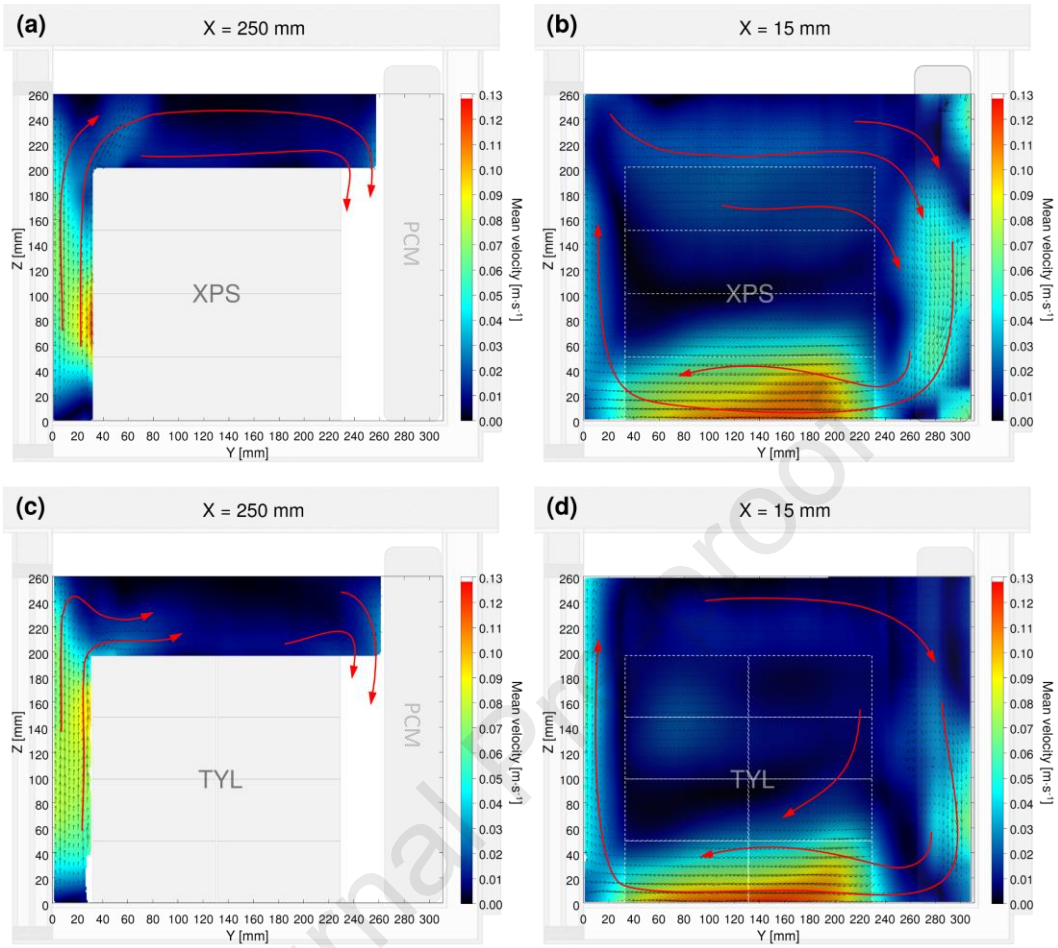

Fig. 10 Air velocity fields at (a and c) the middle (x = 250 mm) and (b and d) the lateral (x = 15 mm) planes of the box with the PCM on the side wall.

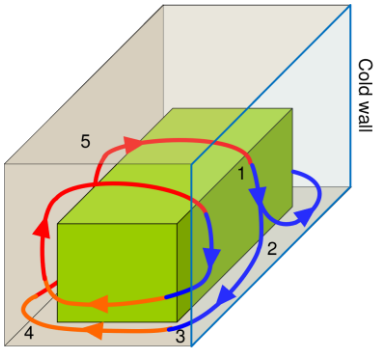

Fig. 11 Illustration of three-dimentional flow in a box with PCM on the side wall. Numbers indicate the states of the flow.

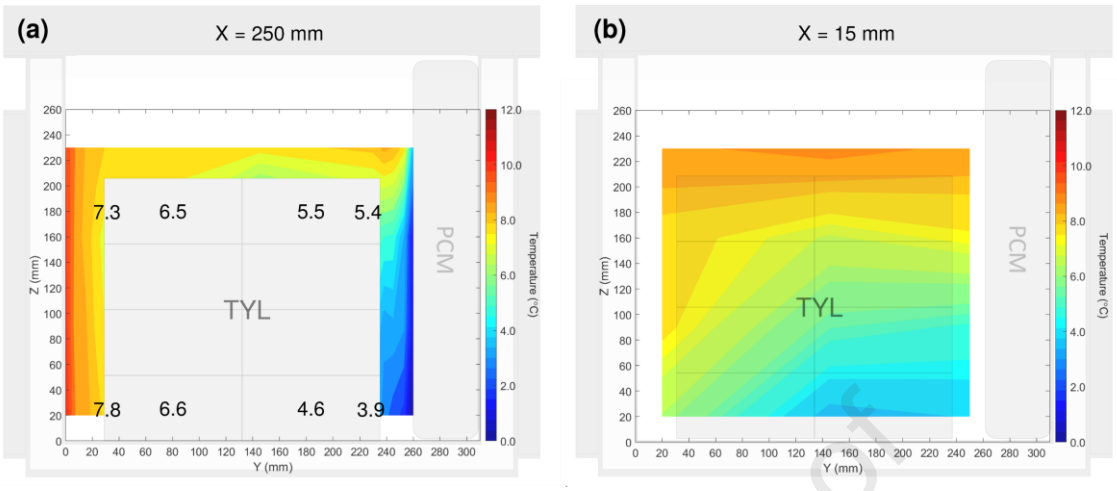

Fig. 12 Air temperature field on (a) the middle (x = 250 mm) and (b) the lateral (x = 15 mm) planes of the box with PCM on the side wall. Values indicate the time-averaged core and surface temperatures of the test products.

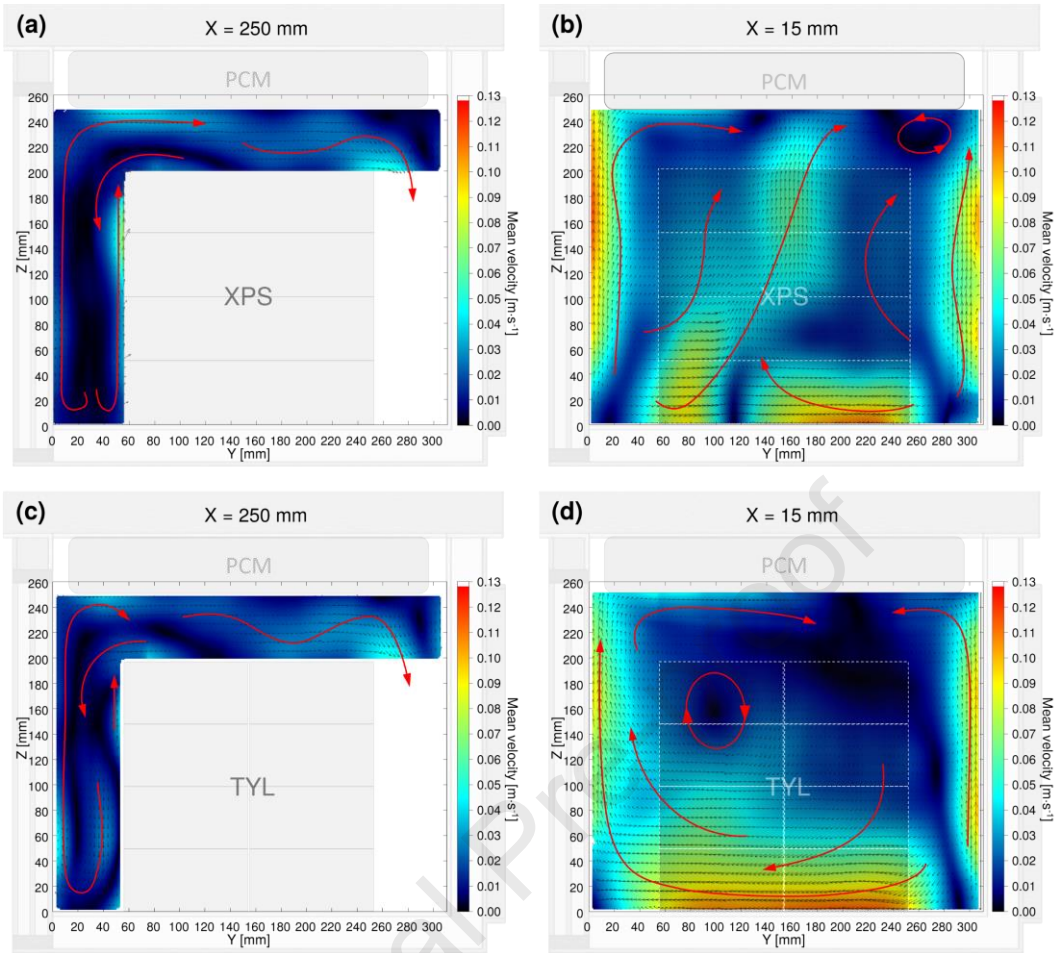

Fig. 13 Air velocity fields on (a and c) the middle (x = 250 mm) and (b and d) the lateral (x = 15 mm) planes of the box equipped with PCM on the lid.

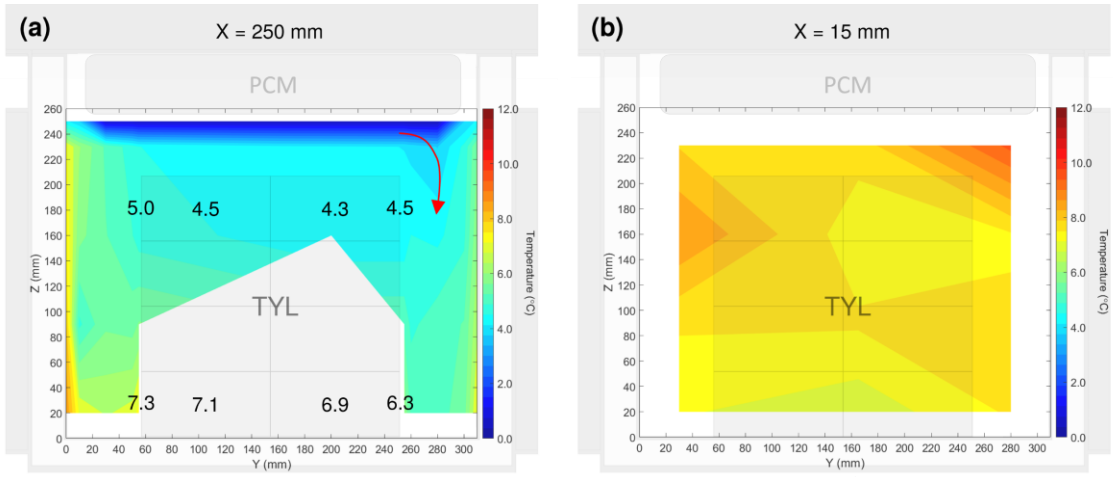

Fig. 14 Air temperature field on (a) the middle (x = 250 mm) and (b) the lateral (x = 15 mm) planes of the box with PCM on the lid. Values indicate the time-averaged core and surface temperatures of the test packs.

Highlights

- Airflow and heat transfer due to natural convection in an insulated box with PCM were studied.
- Effect of PCM positions on flow and temperature fields was investigated.
- The highest observed air velocities in the box were around 0.1 $m \cdot s^{-1}$.
- PCM position exerted no significant effect on maximum product temperature.
- Gaps should be left between the product and the box walls or PCM.

Conflict of Interest and Authorship Conformation Form

Please check the following as appropriate:

☑ All authors have participated in (a) conception and design, or analysis and interpretation of the data; (b) drafting the article or revising it critically for important intellectual content; and (c) approval of the final version.

☑ This manuscript has not been submitted to, nor is under review at, another journal or other publishing venue.

☑ The authors have no affiliation with any organization with a direct or indirect financial interest in the subject matter discussed in the manuscript

☑ The following authors have affiliations with organizations with direct or indirect financial interest in the subject matter discussed in the manuscript.

Author's name	**Affiliation**
Tanathep Leungtongkum	Université Paris-Saclay, INRAE, FRISE, 92761, Antony, France
Onrawee Laguerre	Université Paris-Saclay, INRAE, FRISE, 92761, Antony, France
Denis Flick	Université Paris-Saclay, INRAE, AgroParisTech, UMR SayFood, 91300 Massy, France
Steven Duret	Université Paris-Saclay, INRAE, FRISE, 92761, Antony, France
Alain Denis	Université Paris-Saclay, INRAE, FRISE, 92761, Antony, France
Nattawut Chaomuang	Department of Food Engineering, School of Engineering, King Mongkut's Institute of Technology Ladkrabang, Bangkok, Thailand 10520